Long life Perovskite Nanoplatelet Lasers with high quality factor enabled through engineering degradation pathways

Guohui Li
Taiyuan University of Technology
Huihui Pi
Taiyuan Univsersity of Technology
Yanfu Wei
Taiyuan Univsersity of Technology
Bolin Zhou
Taiyuan Univsersity of Technology
Ya Gao
Taiyuan Univsersity of Technology
Rong Wen
Taiyuan Univsersity of Technology
Yuying Hao
Taiyuan Univsersity of Technology
Han Zhang (hzhang@szu.edu.cn)
Shenzhen University
Beng S. Ong (bong@hkbu.edu.hk)
Hong Kong Baptist University
Yanxia Cui (yanxiacui@tyut.edu.cn)
Taiyuan Univsersity of Technology

Research Article

Keywords: Perovskite, Lasers, Stability, Passivation, Nanoplatelet

Posted Date: December 22nd, 2021

DOI: https://doi.org/10.21203/rs.3.rs-1117916/v1

Abstract

$MAPbI_3$ perovskite has attracted widespread interests for developing low-cost near infrared semiconductor gain media. However, it faces the instability issue under operation conditions, which remains a critical challenge. It is found that the instability of the $MAPbI_3$ nanoplatelet laser comes from the thermal-induced-degradation progressing from the surface defects towards neighboring regions. By using PbI_2 passivation, the defect-initiated degradation is significantly suppressed and the nanoplatelet degrades in a layer-by-layer way, enabling the $MAPbI_3$ laser sustain for 4500 s (2.7×10^7 pulses), which is almost 3 times longer than that of the nanoplatelet laser without passivation. Meanwhile, the PbI_2 passivated $MAPbI_3$ nanoplatelet laser with the nanoplatelet cavity displaying a maximum quality factor up to ~7800, the highest reported for all $MAPbI_3$ nanoplatelet cavities. Furthermore, a high stability $MAPbI_3$ nanoplatelet laser that can last for 8500 s (5.1×10^7 pulses) is demonstrated based on a dual passivation strategy, by retarding the defect-initiated degradation and surface-initiated degradation, simultaneously. This work provides in-depth insights for understanding the operating degradation of perovskite lasers and the dual passivation strategy paves the way for developing high stability near infrared semiconductor laser media.

1. Introduction

Near infrared semiconductor nanolasers are of great significance for integrated optoelectronic chips [1–3]. An efficient gain medium is one of the key components of the near infrared nanolasers [4–6]. The traditional gain media of near infrared lasers are made of inorganic semiconductors, but their quantum efficiencies are low and the growths require critical conditions[3]. Perovskites have attracted considerable interests and been considered as leading candidate gain media for next generation on-chip optical sources, thanks to their outstanding photophysical properties as well as low-cost and promise for electrically driven lasing [7–10]. Among various perovskite materials, the organic-inorganic hybrid materials, with $MAPbI_3$ as a representative, are of particular interesting in the fields of semiconductor lasers as well as solar cells [11,12], light emitting diodes [13], photodetectors [14], etc., due to their large absorption coefficient, exceptionally low trap-state densities, long charge carrier diffusion lengths, and high charge mobilities [15].

In recent years, organic-inorganic hybrid perovskite lasers have achieved rapid progresses. Zhang *et al.* achieved a room temperature $MAPbI_3$ nanoplatelet laser with a lasing threshold of 37 μJ cm^{-2} and a cavity quality factor of 650 through vapor phase deposition method [3]. Zhu *et al.* demonstrated room-temperature lasing using solution processed single-crystalline $MAPbI_3$ nanowires, which showed a lasing threshold down to 220 nJ cm^{-2} and a cavity quality factor Q as high as 3600 [1]. Jia *et al.* demonstrated continuous wave lasing by an $MAPbI_3$ distributed feed-back laser at a substrate temperature of 102 K [16]. In 2020, Qin *et al.* achieved continuous wave pumped lasing with quais-2D phenylethylammonium bromide and 1-naphthylmethylamibe bromide based perovskite media in air at room temperature [17].

Although various inorganic cations have been proposed to replace the organic cation [16,18,19] and different lead-free perovskites materials have also been developed [20–22], their lasing characteristics including the lasing threshold and cavity quality factor performed well below those of the organic-inorganic Pb based counterparts up to now [11,12,23].

However, organic and inorganic hybrid perovskites suffer from instability under operating conditions. It was reported that the temperature of a distributed feedback $MAPbI_3$ laser on sapphire increased by 30 K after pumping for 50 ns and then by 90 K for 1 ms [24]. Such temperature increase can result in thermal-induced-degradation of perovskite crystals. Fan *et al.* found that the crystalline structure gradually evolved from tetragonal $MAPbI_3$ to trigonal layered PbI_2 after the temperature increased to 358 K [25]. Ascribed to the detrimental temperature increase, most of the organic and inorganic hybrid perovskite lasers could not sustain more than 10^7 pulses. For example, the emission intensity of an inkjet-printed $MAPbI_3$ laser on a flexible PET substrate with a nanoimprinted grating in N_2 atmosphere dropped to 90% of its initial value after ~1×10^6 pulses [26]. The $MAPbI_3$ laser with a silica microsphere resonator could sustain by 8.6×10^6 pulses [2]. Similarly, the solution-processed $FAPbBr_3$ microdisk lasers could work stably for 3000 s (3×10^6 pulses) before dropping to 90% of its initial value [27].

From one hand, promoting the operating stability of lasers is one of the constant tasks of laser technology[28]. Although room temperature continuous wave perovskite lasers have been reported[17], one of the major hurdles towards electrically pumped lasers is resistive heating under current injection[7]. On the other hand, improving the thermal stability is of critical importance for achieving electrically pumped perovskite lasers. Until now, great efforts have been made to improve the stability of organic-inorganic perovskites while maintaining the outstanding photophysical properties [29–31]. The encapsulation strategy has been resorted to improve the perovskite lasing stability. For example, a thin poly-methyl-methacrylate (PMMA) encapsulation layer was applied in a $MAPbI_3$ photonic crystal laser so that the operational stability at a pump intensity of 102.5±6.4 μJ/cm^2 being extended from 600 s (10^5 pulses) to 6000 s (10^6 pulses) [32]. By using a CYTOP encapsulation film, a $MAPbI_3$ distributed feedback laser that operated at a pump intensity of 7 μJ/cm^2 could sustain 10^7 pulses before dropping to 90% of its initial value [33]. It was also demonstrated that the stability of $MAPbI_3$ could be improved by encapsulating with boron nitride flakes [25]. Nevertheless, the stability performance of hybrid perovskite lasers is still dissatisfactory, and the microscopic degradation mechanism for the hybrid perovskite during the laser pumping process remains unknown.

In this work, by continuously monitoring the emission properties of a $MAPbI_3$ nanoplatelet laser, we find that the gradual degradation of tetragonal $MAPbI_3$ starts from the surface defects and the laser output intensity drops to 90% after ~1200 s (7.2×10^6 pulses). Those surface defects on the $MAPbI_3$ nanoplatelets can be effectively passivated by introducing excess PbI_2. As a result, the evolution from tetragonal $MAPbI_3$ to PbI_2 launches from the crystal surface and the nanoplatelet degrades layer-by-layer,

bringing forward the operational stability being extended from 1200 s to 4500 s (2.7×10^7 pulses). On the basis of the PbI_2 passivated nanoplatelet, we further introduce an additional DBP ($C_{64}H_{36}$) protection film, which can suppress the surface initiated degradation by passivating the surface dangling bonds, thereby dramatically improving the operational stability of the $MAPbI_3$ laser to up to 8500 s (5.1×10^7 pulses), which is around 1.89 times as long as that of the $MAPbI_3$ nanoplatelet with only PbI_2 passivation. Compared with the initial $MAPbI_3$ nanoplatelets with surface defects, the dual passivation strategy with both PbI_2 and DBP enables the $MAPbI_3$ laser sustain 6 times longer, promoting the stability performances of $MAPbI_3$ perovskite lasers significantly. The present passivation strategy of improving the perovskite laser stability paves the way on developing high stability near infrared gain media. In addition, our first attempt on demonstrating the degradation mechanism of the hybrid perovskite crystals under laser pumping might provide in-depth insights for resolving the critical stability hurdle in practical applications of perovskite lasers.

2. Results And Discussions

The $MAPbI_3$ nanoplatelets used in our study were synthesized by the two-step chemical vapor deposition method, that includes the first step of growing PbI_2 nanoplatelets and the second step of converting PbI_2 nanoplatelets into $MAPbI_3$ nanoplatelets [34]. During the operational stability measurement, we continuously monitored the emission properties and the spectra of the $MAPbI_3$ nanoplatelet laser in ambient air condition with a pumping density of 26.1 μJ/cm^2 ($1.1P_{th}$).

As can be seen in Fig. 1a, the emission intensity was almost uniform on the surface of the nanoplatelet laser during the first 600 s. After operating for 800 s, the emission intensity on the left side of the nanoplatelet laser started to decrease. Since the measurement takes long time, the emission intensity of the laser operating at a pump density of $1.1P_{th}$ (26.1 μJ/cm^2) during the operating time were measured using an ideaoptics PG2000-Pro spectrometer(See stability characteristic section for more information) as shown in Fig. 1b. As can be seen, the laser output intensity as a whole does not change, because more pumping energy can reach lower $MAPbI_3$ layer, that keeps the population inversion ΔN required for maintaining the output intensity $I \propto \Delta N$ almost unchanged as the upper layer of $MAPbI_3$ degrades; see supporting information for more details. After operating for 1100 s, the emission intensity on a small area on the left side of the nanoplatelet laser decreases dramatically and the area almost becomes dark. After operating for 1200 s (7.2×10^6 pulses), the dark area increases as shown in Fig. 1a and the output intensity of the nanoplatelet laser decreases to 90% of the initial intensity as can be seen in Fig. 1b. The operational stability data is in agreement with most of the reported $MAPbI_3$ lasers [1,2,35]. After operating for 1400 s, the dark area keeps increasing and the output intensity of the nanoplatelet laser decreases dramatically. The laser dies after working for 1750 s. Besides this nanoplatelet laser, the operational stability of another two unpassivated nanoplatelet lasers has also been measured. The two nanoplatelet lasers can sustain for 1170 s (Fig. S1a) and 1200 s (Fig. S1b) before output intensity decreases to 90% of their initial value which are consistent with that of the first nanoplatelet laser.

The emission spectrum evolutions of the laser operating at a pump density of 1.1P_{th} (26.1 μJ/cm^2) during the operating time were also measured by using an ideaoptics PG2000-Pro spectrometer (See stability characteristic section for more information). From the emission spectrum as shown in Fig. 1c, we can see that the intensity of the laser line after operating for 1000 s starts to decrease with the decreasing spontaneous emission intensity. After 1700 s, the spontaneous emission intensity drops down to 50% of its initial intensity and the laser line almost disappears at the same time (see in Fig. S2). As can be seen in the microscopic image (Fig. 1d) of the $MAPbI_3$ nanoplatelet after operating for 1800 s, some parts of the nanoplatelet have faster degradations and the color of these parts have changed to brown as compared with the yellow color of the rest regions.

From the microscopic image of the initial $MAPbI_3$ nanoplatelet as shown in Fig. 1e, it is seen that the nanoplatelet with a thickness of ~ 130 nm (see in Fig. S3) initially has a uniform surface and the color of the whole surface is almost the same. However, from the scanning electron microscopy (SEM) images of the $MAPbI_3$ nanoplatelets, some surface defects are found on the surface as can be seen Fig. 1e. The atomic force microscopy (AFM) images (Fig. 1f) of the nanoplatelets shows that the RMS roughness of the surface is ~2.1 nm. Therefore, the $MAPbI_3$ nanoplatelet under operating condition starts to degrade from the surface defects and progress gradually to neighboring areas as shown in Fig. 1a. The corresponding X-ray diffraction (XRD) pattern shows that initially the perovskites nanoplatelets has a pure tetragonal $MAPbI_3$ crystal structure without impurities such as PbI_2 (see in Fig. S4). The existence of the small (202), (112), (210), and (221) peaks indicate that the $MAPbI_3$ nanoplatelets are in the room-temperature tetragonal phase [36]. After operating for 1800 s, more than a half of the surface has changed from yellow to brown as can be seen in Fig. 1d. The corresponding XRD pattern shows that (001), (003), and (004) peaks of PbI_2 appears after the nanoplatelets operating for 1800 s, confirming that some part of the tetragonal phase $MAPbI_3$ nanoplatelet degrades to PbI_2 [36].

The observed phenomenon of $MAPbI_3$ degradation launching from the surface defects deviates from the layer-by-layer degradation theory, which expresses that the thermal-induced-degradation starts from the surface of $MAPbI_3$ as a result of dangling bonds, structure relaxation and charge redistribution on the surface and happens in a sequential layer-by-layer style [25]. A calculation of the transient thermal response of a $MAPbI_3$ nanoplatelet shows that, with a moderate laser pump density of ~17 μJ/cm^2, the transient temperature at the nanoplatelet (see in Fig. S6) far exceeds the thermal degradation threshold temperature [25]. It is unquestionable that the $MAPbI_3$ nanoplatelet suffers detrimental thermal-induced-degradation in the experiment. In reality, with respect to the smooth flat surface, the surface defect regions on the surface of the nanoplatelet can form extra dangling bonds on their walls, which initiate new degradation pathways. Since the longer Pb-I-Pb bonds along the [001] direction of $MAPbI_3$ are less resistance to bond breakage than those in the (001) plane[37], these bonds tend to break first under external stimulus and form dangling bonds. The region with more defects on the nanoplatelet, the faster the speed of the thermal-induced-degradation. Under laser operating conditions, the expansion of the defect region would accelerate the degradation, so a snowball effect is produced. Therefore, ascribed to

the existence of surface defects, the degradation proceeds from the inner part to the edge rather than following the layer-by-layer degradation theory. It is plausible to suppose that reducing the defects can suppress the degradation and making the nanoplatelet lasers operating for longer times.

In contrast to fully converting PbI_2 to $MAPbI_3$ during the second step of chemical vapor deposition, a certain amount of PbI_2 was intentionally reserved to passivate the defects in fabrication of new perovskite nanoplatelets. As shown in Fig. 2a, $MAPbI_3$ nanoplatelets with well-defined triangular and hexagonal shape and 100-200 nm thickness and tens of micrometers edge lengths were synthesized [34]. As can be seen in the XRD pattern (Fig. 2b), there also exist (001), (003) and (004) peaks of the PbI_2 structure in addition to the tetragonal phase $MAPbI_3$ peaks, confirming the excess PbI_2 being reserved in the perovskites nanoplatelets. Fig. 2c shows the microscopic image of the $MAPbI_3$ nanoplatelet for carrying out the following lasing operation. The perovskite nanoplatelet has a thickness of ~ 180 nm (see in Fig. S7). The SEM image in Fig. 2d reflects that the surface defects were successfully passivated to a large extent. As can be seen, a newly formed species appeared on the nanoplatelet surface and the new species displayed brighter color as compared with neighboring species as a result of poorer conductivity [38]. According to the XRD pattern as shown in Fig. 2b, the species should be PbI_2, while the darker films are considered to be perovskite. Here, the unreacted PbI_2, without destroying the perovskite crystal structure, is of great helpful for reducing the surface defects in the $MAPbI_3$ nanoplatelets. The AFM image in Fig. 2e indicates a RMS roughness of ~ 0.7 nm, confirming that the nanoplatelets have much smoother surfaces supporting the whispering-gallery-mode cavity after passivation.

The influence of excess PbI_2 on the laser performance are investigated in the following. The light-in-light-out curve in Fig. 2f shows that the emission intensity grows slowly with the increasing pump density below the pump density of ~14.98 μJ/cm^2, and then the emission intensity grows very quickly. At a pump intensity of 15.87 μJ/cm^2, the emission intensity saturate due to blue shift of center wavelength of the laser[1]. Lasing death did not happen in the measurement. Here, the lasing threshold of ~14.98 μJ/cm^2 is lower than that of the $MAPbI_3$ nanoplatelet laser without passivation. Since the spectrum has a narrow linewidth which cannot resolved by ideaoptics PG2000-Pro spectrometer, the emission spectrum evolutions of the laser operating at a different pump density were measured by using a Horiba iHR 550 spectrometer(See optical spectrum characterization section for more information). The spectra of the emission light in Fig. 2g show that there exists only spontaneous emission below 14.98 μJ/cm^2. Above the threshold, a narrow laser peak appears and the laser peak increases rapidly with the increasing of pump density. As shown in Fig. 2h, separation between adjacent modes is ~0.3 nm which is in agreement with the theoretical value (~0.3 nm) calculated with edge length of the cavity[34]. Lorentz fit of the laser peak at the pump density of 14.98 μJ/cm^2 shows that the full-width at half-maximum (FWHM) is ~0.1 nm which corresponds to a cavity quality factor Q of 7810, much superior to the values of all reported $MAPbI_3$ nano-laser (the highest reported Q of 3600 belonged to the state-of-the-art $MAPbI_3$ nanowire laser cavity [1]).

We also measured the time-resolved photo-luminescence as shown in Fig. 2i. Since $MAPbI_3$ crystals show both fast dynamics and slow dynamics, biexponential fitting were performed to quantify the carrier dynamics. Here, the slow decay component reveals the lifetime of carriers[39]. At a pump density of 11.12 $\mu J/cm^2$ (below threshold), the PL decay curve shows a long average lifetime of ~6.62 ns. At a pump density of 24.8 $\mu J/cm^2$ (above the threshold), the PL decay curve shows a short average lifetime of ~0.67 ns. It can be concluded that the lasing threshold has been reduced and quality factor of nanoplatelet cavities has been improved significantly thanks to the reduced surface defects by PbI_2 passivation.

Operational stability of the PbI_2 passivated $MAPbI_3$ nanoplatelet laser has also been tested under continuous laser pumping with a pumping density of 16.5 $\mu J/cm^2$ ($P = 1.1P_{th}$). As can be seen in Fig. 3a, the laser emission intensity of the PbI_2 passivated laser is very stable for 4600 s. After 4600 s, the laser output intensity decreases very rapidly and the emission from surface becomes weak as a whole. After operating for 5600 s, its surface color was still uniform as shown by the microscopic image of the nanoplatelet in Fig. 3b. Thanks to PbI_2 passivation, the surface defects are reduced significantly and thereby the surface defects induced degradation are effectively suppressed. Therefore, on the surface of the nanoplatelet, there only exists the dangling bonds triggered thermal decomposition, and correspondingly, the degradation starts from the surface and proceeds layer-by-layer; see supporting information for more details. Since the measurement takes long time, the emission intensity of the laser operating at a pump density of $1.1P_{th}$ (16.48 $\mu J/cm^2$) during the operating time were also measured by using an ideaoptics PG2000-Pro spectrometer which is capable of long-time measurement (See stability characteristic section for more information). As can be seen in Fig. 3c, the monitoring of the laser emission intensity shows that the laser can maintain 90% of the initial intensity after 4500 s (2.7×10^7 pulses), which is nearly 3 times longer than that of the $MAPbI_3$ nanoplatelet laser without passivation, and is 2.7 times longer than that of the state of the art $MAPbI_3$ nanowire laser [1]. Besides this PbI_2 passivated nanoplatelet laser, the operational stability of another two PbI_2 passivated nanoplatelet lasers has also been measured. The two nanoplatelet lasers can sustain for 4400 s (Fig. S8a) and 4300 s (Fig. S8b) before output intensity decreases to 90% of their initial value which are consistent with that of the first PbI_2 passivated nanoplatelet laser.

Next, we optimized the operational stability of PbI_2 passivated $MAPbI_3$ nanoplatelet laser by introducing an additional encapsulation layer to passivate the surface of the nanoplatelet. The surface-imitated layer-by-layer degradation of $MAPbI_3$ is considered to be caused by Pb and I dangling bonds on the $MAPbI_3$ surface. Hydrogen and pseudo-hydrogen atoms are supposed to provide an ideal passivation to pair the electron in the dangling bonds on the surface of semiconductor nano-structures [40, 41]. DBP ($C_{64}H_{36}$) is a promising material for improving the performances of perovskite optoelectronic devices such as solar cells and light emitting diodes [42, 43].

To suppress the surface-imitated degradation of perovskite nanoplatelets, we employed a thin DBP film as the encapsulation layer on newly synthesized PbI_2 passivated $MAPbI_3$ nanoplatelet surface to form a

DBP-$MAPbI_3$-mica heterostructure as shown in Fig. 4a. The DBP film was spin-coated on the surface of $MAPbI_3$ nanoplatelets on mica substrate as shown in Fig. 4b. After coating the DBP film, the $MAPbI_3$ nanoplatelets on mica substrate (Fig. S9a) become darker as compared with the uncoated $MAPbI_3$ nanoplatelets on mica substrate (Fig. S9b). Without passivation, the $MAPbI_3$ surface with Pb and I dangling bonds is more susceptible to degrade. As shown in Fig. S10, the yellow nanoplatelet degrades severely for 48 h in ambient air condition. Instead, the DBP encapsulated nanoplatelet can keep in ambient air condition for more than 120 h as can be seen in Fig. S11. That is because, with DBP encapsulation, the H^- in the $C_{64}H_{36}$ interact with perovskite surface dangling bonds, which effectively reduces the surface activity and enables a highly stable $MAPbI_3$ nanoplatelet.

The lasing performances of the DBP encapsulated $MAPbI_3$ nanoplatelet laser are shown in Fig. 4. It is found that the lasing threshold (~16.32 μJ/cm^2) of $MAPbI_3$ nanoplatelet laser is slightly increased by DBP encapsulation as shown in Fig. 4c, which might be induced by light absorption of DBP. Since the spectrum has a narrow linewidth which cannot resolved by ideaoptics PG2000-Pro spectrometer, the emission spectrum evolutions of the laser operating at a different pump density were also measured by using a Horiba iHR 550 spectrometer (See optical spectrum characterization section for more information). The spectra of the emission light in Fig. 4d show that there exists only spontaneous emission below 16.32 μJ/cm^2. Above the threshold, a narrow laser peak appears and the laser peak increases rapidly with the increasing of pump density. As can be seen in Fig. 4e, Lorentz fit of the laser peak at the pump density of 16.47 μJ/cm^2 shows that the FWHM is ~0.1 nm which corresponds to a cavity quality factor Q of ~ 7799.

We then performed the operational stability test of the obtained stable $MAPbI_3$ nanoplatelet at a pump density of 1.1P_{th} (~17.95 μJ/cm^2) at room temperature in ambient air condition. Since the measurement takes long time, the emission intensity of the laser was measured by using an ideaoptics PG2000-Pro spectrometer (See stability characteristic section for more information). As can be seen in Fig. 4f, it shows that the dual passivation processed $MAPbI_3$ nanoplatelet laser have considerably improved operational stability. The output intensity of the dual passivation processed laser keeps 9 % of the initial value for longer than 8500 s (5.1×10^7 pulses), which is around 1.89 times as long as that of the $MAPbI_3$ nanoplatelet with only PbI_2 passivation. Compared with the initial unpassivated $MAPbI_3$ nanoplatelets with surface defects, the dual passivation strategy enables the $MAPbI_3$ laser sustains 6 times longer, outperforming the performances of all reported hybrid perovskite lasers. Its operational stability is even better than some of the all inorganic $CsPbBr_3$ lasers [16,44]. This result confirms that the rich hydrogen atoms contained in the DBP molecules can provide effective passivation of the electron in the dangling bonds on the surface of $MAPbI_3$ nanoplatelets. Besides this dual passivation processed nanoplatelet laser, the operational stability of another two dual passivation processed nanoplatelet lasers has also been measured. The two nanoplatelet lasers can sustain for 8290 s (Fig. S12a) and 8390 s (Fig. S12b) before output intensity decreases to 90% of their initial value which are consistent with that of the first dual passivation processed nanoplatelet laser.

The average operation time of unpassivated (sample A), PbI_2 passivated (sample B) and dual passivation processed nanoplatelet lasers (sample C) under femtosecond laser pumping with a repetition rate of 6 kHz in ambient air condition are 1190 s, 4400 s and 8450 s (see Fig. S13), respectively. It can be seen that the average operation time of PbI_2 passivated nanoplatelet lasers is more than three times longer than that of the unpassivated nanoplatelet lasers. Through dual passivation processing, the average operation time of nanoplatelet lasers is improved more than seven times as compared with that of the unpassivated nanoplatelet lasers.

In conclusion, a high stability $MAPbI_3$ nanoplatelet laser has been demonstrated based on a dual passivation strategy, in which excess PbI_2 and a DBP encapsulation film were utilized to passivate the defect-initiated degradation and the surface-initiated degradation, respectively. The continuous monitoring of the emission intensity of the initial $MAPbI_3$ nanoplatelet laser reflects that the laser instability stems from the thermal-induced-degradation which starts at the surface defects on the surface of $MAPbI_3$ and then progresses towards the neighboring regions. Unreacted PbI_2 has been employed to successfully suppress the defect-induced-degradation, therefore the nanoplatelet degrades in a layer-by-layer way. As a result, the PbI_2 passivated nanoplatelet laser can sustain for 4500 s (2.7×10^7 pulses), which is more than 3 times longer than the nanoplatelet laser without passivation. It has been demonstrated that the PbI_2 passivated nanoplate laser has a threshold as low as 14.98 $\mu J/cm^2$ and a cavity quality factor up to ~7810. To further retard the surface-initiated degradation, an additional DBP film has been utilized as a protection layer on the PbI_2 passivated $MAPbI_3$ nanoplatelet. The DBP encapsulated nanoplatelet show considerably improved operational stability which can last for 8500 s (5.1×10^7 pulses) until it falls to 90% of its initial intensity. Our results demonstrate the microscopic degradation mechanism of a $MAPbI_3$ nanoplatelet laser and show the critical importance of managing the defects and dangling bonds of the surface in developing stable perovskite near infrared lasers.

Methods

Synthesis of Perovskite NPLs: PbI_2 (99.999%, Alfa) was used as a single source and placed into a quartz tube mounted on a single zone furnace (CY scientific instrument, CY-O1200-1L) at a room temperature of 18°C. The fresh-cleaved muscovite mica substrate was pre-cleaned with acetone and placed in the downstream region inside the quartz tube. The quartz tube was first evacuated to 0.1 Pa, followed by a 30 sccm flow of high purity Ar premixed with 10% H_2 gas. The temperature and pressure inside the quartz tube were set and stabilized at 380°C and 0.12 MPa for PbI_2. The synthesis of PbI_2 was completed within 14 min, and the furnace was allowed to cool naturally to room temperature. Then, pre-grown lead halide nanoplatelets were thermally intercalated with MAI (Xi'an Polymer light technology) in a fresh quartz tube. The mica substrate with nanoplatelets was placed in the downstream region, while the MAI powder was placed in the center of the tube. The intercalation was carried out at 120°C at a pressure of 0.11 MPa with a 34-sccm flow of high purity Ar for 200 min to convert the lead halides to perovskites completely.

For PbI_2 passivation, the intercalation was carried out for 170 min to keep parts of lead iodide for passivation.

Fabrication of the DBP film. 0.002 g DBP (99%, Han Feng) was first fully dissolved in 1 mL chlorobenzene (Sigma). After filtration, 20 mL DBP solution was spin-coated on the surface of the perovskite nanoplatelets at 4500 rpm for 30 s in an N_2 filled glovebox. The film formed after 2 min.

Image and phase characterizations. The optical images of $MAPbI_3$ nanostructures were obtained on a Nikon LV150 optical microscope. The AFM images were collected on an FM-Nanoview 1000 AFM (FSM Precision) which samples 512 points separately in x and y direction. The XRD data were acquired on a DX-2700 diffractometer (Dandong Haoyuan) by using a sampling time of 0.1 s. The SEM images were obtained at an accelerating voltage of 5.0 kV by using a JEOL JSM-IT500 scanning electron microscope.

Optical spectrum characterization. We carried out optically pumped lasing measurements on a home-built microscope setup. The 343 nm excitation pulses were generated by frequency tripling the 1028 nm output (with a BBO crystal) from a Light Conversion Carbide Femtosecond laser (290 fs, 6 kHz, 1028 nm). The pumping source was focused onto samples via an uncoated convex lens (Focal length: 20 cm, Transmittance: 80%). To ensure uniform energy injection, the laser spot diameter was focused to ~107 μm. The transmitted emission was collected through a 20× objective lens (Olympus, Numerical Aperture: 0.4). Half of the emission signals were imaged on a camera (Hamamatsu, C11440-36U). The other half of the emission signal from a single nanoplatelet was collected into an optical fiber with core diameter of 600 mm and analyzed using a Horiba iHR 550 equipped with a symphony CCD head. Each spectrum was obtained through a single measurement. The CCD head has a E2V manufactured 2048×512 pixel Back Illuminated Visible CCD chip and was cooled to 140 K with liquid N_2. The spectrometer can work stably for 4 h after filled with liquid N_2. A 1200 g/mm, 500 nm blazed, 76 mm×76 mm, and ion-etched holographic diffraction grating and the entrance slit of 50 μm were used in the measurement. The spectral resolution of the spectrometer is ~ 0.04 nm. The emission was time-resolved by using a TCSPC module (Picoquant, PicoHarp 300) and a SPAD detector (MPD, PD-100-CTE) with an instrument response function of 30 ps (FWHM).

Stability characterization. The emission intensity from a single nanoplatelet was monitored using an ideaoptics PG2000-Pro spectrometer with a wavelength resolution (FWHM) of 0.3 nm in the range 700-900 nm. Since the spectrometer does not require cooling liquid, it can work stably for longer times. For spectral range of 200-1100 nm, the ideaoptics PG2000 spectrometer with a wavelength resolution (FWHM) of 1.3 nm was used.

Declarations

Acknowledgements

This work was supported by the National Natural Science Foundation of China (61922060, 61775156, 61961136001 and 61875138). The commercialization cultivation program of Shanxi college research findings (2020CG013). YC also acknowledges support from Key Research and Development (International Cooperation) Program of Shanxi Province (201803D421044), Henry Fok Education Foundation Young Teachers fund, and Platform and Base Special Project of Shanxi Province (201805D131012-3). HZ also acknowledges support from the Nature Science Foundation of Guangdong Province (2018A030313401), Shenzhen Nanshan District Pilotage Team Program (LHTD20170006), and the Science and Technology Innovation Commission of Shenzhen (JCYJ20170811093453105, JCYJ20170818141519879).

Competing interests

The authors declare no competing interests.

References

1 Zhu, H. *et al.* Lead halide perovskite nanowire lasers with low lasing thresholds and high quality factors. *Nature Materials* **14**, 636, doi:10.1038/nmat4271 https://www.nature.com/articles/nmat4271#supplementary-information (2015).

2 Sutherland, B. R., Hoogland, S., Adachi, M. M., Wong, C. T. O. & Sargent, E. H. Conformal Organohalide Perovskites Enable Lasing on Spherical Resonators. *ACS Nano* **8**, 10947-10952, doi:10.1021/nn504856g (2014).

3 Zhang, Q., Ha, S. T., Liu, X., Sum, T. C. & Xiong, Q. Room-Temperature Near-Infrared High-Q Perovskite Whispering-Gallery Planar Nanolasers. *Nano Letters* **14**, 5995-6001, doi:10.1021/nl503057g (2014).

4 Hill, M. T. & Gather, M. C. Advances in small lasers. *Nature Photonics* **8**, 908, doi:10.1038/nphoton.2014.239 https://www.nature.com/articles/nphoton.2014.239#supplementary-information (2014).

5 Wei, Q. *et al.* Recent Progress in Metal Halide Perovskite Micro- and Nanolasers. *Advanced Optical Materials* **0**, 1900080, doi:10.1002/adom.201900080 (2019).

6 Wang, K., Wang, S., Xiao, S. & Song, Q. Recent Advances in Perovskite Micro- and Nanolasers. *Advanced Optical Materials* **6**, 1800278, doi:10.1002/adom.201800278 (2018).

7 Sutherland, B. R. & Sargent, E. H. Perovskite photonic sources. *Nature Photonics* **10**, 295, doi:10.1038/nphoton.2016.62 (2016).

8 Zhang, Y. *et al.* Photonics and optoelectronics using nano-structured hybrid perovskite media and their optical cavities. *Physics Reports* **795**, 1-51, doi:https://doi.org/10.1016/j.physrep.2019.01.005

(2019).

9 Schlaus, A. P. *et al.* How lasing happens in CsPbBr3 perovskite nanowires. *Nature Communications* **10**, 265, doi:10.1038/s41467-018-07972-7 (2019).

10 Liu, Y. *et al.* Efficient blue light-emitting diodes based on quantum-confined bromide perovskite nanostructures. *Nature Photonics* **13**, 760-764, doi:10.1038/s41566-019-0505-4 (2019).

11 Green, M. *et al.* Solar cell efficiency tables (version 57). *Progress in Photovoltaics: Research and Applications* **29**, 3-15, doi:https://doi.org/10.1002/pip.3371 (2021).

12 Chen, Y. *et al.* Dual Passivation of Perovskite and SnO2 for High-Efficiency MAPbI3 Perovskite Solar Cells. *Advanced Science* **n/a**, 2001466, doi:https://doi.org/10.1002/advs.202001466 (2021).

13 Veldhuis, S. A. *et al.* Perovskite Materials for Light-Emitting Diodes and Lasers. *Advanced Materials* **28**, 6804-6834, doi:10.1002/adma.201600669 (2016).

14 Li, G. *et al.* High detectivity photodetectors based on perovskite nanowires with suppressed surface defects. *Photon. Res.* **8**, 1862-1874, doi:10.1364/PRJ.403030 (2020).

15 Manser, J. S., Christians, J. A. & Kamat, P. V. Intriguing Optoelectronic Properties of Metal Halide Perovskites. *Chemical Reviews* **116**, 12956-13008, doi:10.1021/acs.chemrev.6b00136 (2016).

16 Tang, B. *et al.* Single-Mode Lasers Based on Cesium Lead Halide Perovskite Submicron Spheres. *ACS Nano* **11**, 10681-10688, doi:10.1021/acsnano.7b04496 (2017).

17 Qin, C. *et al.* Stable room-temperature continuous-wave lasing in quasi-2D perovskite films. *Nature* **585**, 53-57, doi:10.1038/s41586-020-2621-1 (2020).

18 Eaton, S. W. *et al.* Lasing in robust cesium lead halide perovskite nanowires. *Proceedings of the National Academy of Sciences* **113**, 1993, doi:10.1073/pnas.1600789113 (2016).

19 Zhao, C. *et al.* Stable Two-Photon Pumped Amplified Spontaneous Emission from Millimeter-Sized CsPbBr3 Single Crystals. *The Journal of Physical Chemistry Letters* **10**, 2357-2362, doi:10.1021/acs.jpclett.9b00734 (2019).

20 Ju, M.-G. *et al.* Toward Eco-friendly and Stable Perovskite Materials for Photovoltaics. *Joule* **2**, 1231-1241, doi:https://doi.org/10.1016/j.joule.2018.04.026 (2018).

21 Yan, Y., Pullerits, T., Zheng, K. & Liang, Z. Advancing Tin Halide Perovskites: Strategies toward the ASnX3 Paradigm for Efficient and Durable Optoelectronics. *ACS Energy Letters* **5**, 2052-2086, doi:10.1021/acsenergylett.0c00577 (2020).

22 Luo, J. *et al.* Efficient and stable emission of warm-white light from lead-free halide double perovskites. *Nature* **563**, 541-545, doi:10.1038/s41586-018-0691-0 (2018).

23 Jeong, M. *et al.* Stable perovskite solar cells with efficiency exceeding 24.8% and 0.3-V voltage loss. *Science* **369**, 1615, doi:10.1126/science.abb7167 (2020).

24 Jia, Y., Kerner, R. A., Grede, A. J., Rand, B. P. & Giebink, N. C. Factors that Limit Continuous-Wave Lasing in Hybrid Perovskite Semiconductors. *Advanced Optical Materials* **8**, 1901514, doi:10.1002/adom.201901514 (2020).

25 Fan, Z. *et al.* Layer-by-Layer Degradation of Methylammonium Lead Tri-iodide Perovskite Microplates. *Joule* **1**, 548-562, doi:https://doi.org/10.1016/j.joule.2017.08.005 (2017).

26 Mathies, F. *et al.* Inkjet-printed perovskite distributed feedback lasers. *Opt. Express* **26**, A144-A152, doi:10.1364/OE.26.00A144 (2018).

27 Li, X. *et al.* Stable Whispering Gallery Mode Lasing from Solution-Processed Formamidinium Lead Bromide Perovskite Microdisks. *Advanced Optical Materials* **8**, 2000030, doi:https://doi.org/10.1002/adom.202000030 (2020).

28 Zhang, Q., Shang, Q., Su, R., Do, T. T. H. & Xiong, Q. Halide Perovskite Semiconductor Lasers: Materials, Cavity Design, and Low Threshold. *Nano Letters* **21**, 1903-1914, doi:10.1021/acs.nanolett.0c03593 (2021).

29 Li, G. *et al.* Stability of Perovskite Light Sources: Status and Challenges. *Advanced Optical Materials* **8**, 1902012, doi:https://doi.org/10.1002/adom.201902012 (2020).

30 Leijtens, T. *et al.* Stability of Metal Halide Perovskite Solar Cells. *Advanced Energy Materials* **5**, 1500963, doi:https://doi.org/10.1002/aenm.201500963 (2015).

31 Fu, Q. *et al.* Recent Progress on the Long-Term Stability of Perovskite Solar Cells. *Advanced Science* **5**, 1700387, doi:10.1002/advs.201700387 (2018).

32 Chen, S. *et al.* A Photonic Crystal Laser from Solution Based Organo-Lead Iodide Perovskite Thin Films. *ACS Nano* **10**, 3959-3967, doi:10.1021/acsnano.5b08153 (2016).

33 Whitworth, G. L. *et al.* Nanoimprinted distributed feedback lasers of solution processed hybrid perovskites. *Opt. Express* **24**, 23677-23684, doi:10.1364/OE.24.023677 (2016).

34 Li, G. *et al.* Record-Low-Threshold Lasers Based on Atomically Smooth Triangular Nanoplatelet Perovskite. *Advanced Functional Materials* **29**,doi:10.1002/adfm.201805553 (2019).

35 Whitworth, G. L. *et al.* Nanoimprinted distributed feedback lasers of solution processed hybrid perovskites. *Opt Express* **24**, 23677-23684, doi:10.1364/OE.24.023677 (2016).

36 Ha, S. T. *et al.* Synthesis of Organic–Inorganic Lead Halide Perovskite Nanoplatelets: Towards High-Performance Perovskite Solar Cells and Optoelectronic Devices. *Advanced Optical Materials* **2**, 838-

844, doi:https://doi.org/10.1002/adom.201400106 (2014).

37 Brivio, F., et al., Lattice dynamics and vibrational spectra of the orthorhombic, tetragonal, and cubic phases of methylammonium lead iodide. *Physical Review B* **92**,doi:10.1103/PhysRevB.92.144308 (2015).

38 Chen, Q. *et al.* Controllable Self-Induced Passivation of Hybrid Lead Iodide Perovskites toward High Performance Solar Cells. *Nano Letters* **14**, 4158-4163, doi:10.1021/nl501838y (2014).

39 Shi, D. *et al.* Low trap-state density and long carrier diffusion in organolead trihalide perovskite single crystals. *Science* **347**, 519, doi:10.1126/science.aaa2725 (2015).

40 Li, J., Wei, S.-H. & Wang, L.-W. Stability of the DX^- Center in GaAs Quantum Dots. *Physical Review Letters* **94**, 185501, doi:10.1103/PhysRevLett.94.185501 (2005).

41 Li, J. & Wang. Comparison between Quantum Confinement Effects of Quantum Wires and Dots. *Chemistry of Materials* **16**, 4012-4015, doi:10.1021/cm0494958 (2004).

42 Ding, S. *et al.* Enhanced performance of perovskite solar cells by the incorporation of the luminescent small molecule DBP: perovskite absorption spectrum modification and interface engineering. *Journal of Materials Chemistry C* **7**, 5686-5694, doi:10.1039/C9TC00064J (2019).

43 Kirchhuebel, T. *et al.* Self-Assembly of Tetraphenyldibenzoperiflanthene (DBP) Films on Ag(111) in the Monolayer Regime. *Langmuir* **32**, 1981-1987, doi:10.1021/acs.langmuir.5b04069 (2016).

44 Wang, Y. *et al.* All-Inorganic Colloidal Perovskite Quantum Dots: A New Class of Lasing Materials with Favorable Characteristics. *Advanced Materials* **27**, 7101-7108, doi:https://doi.org/10.1002/adma.201503573 (2015).

Figures

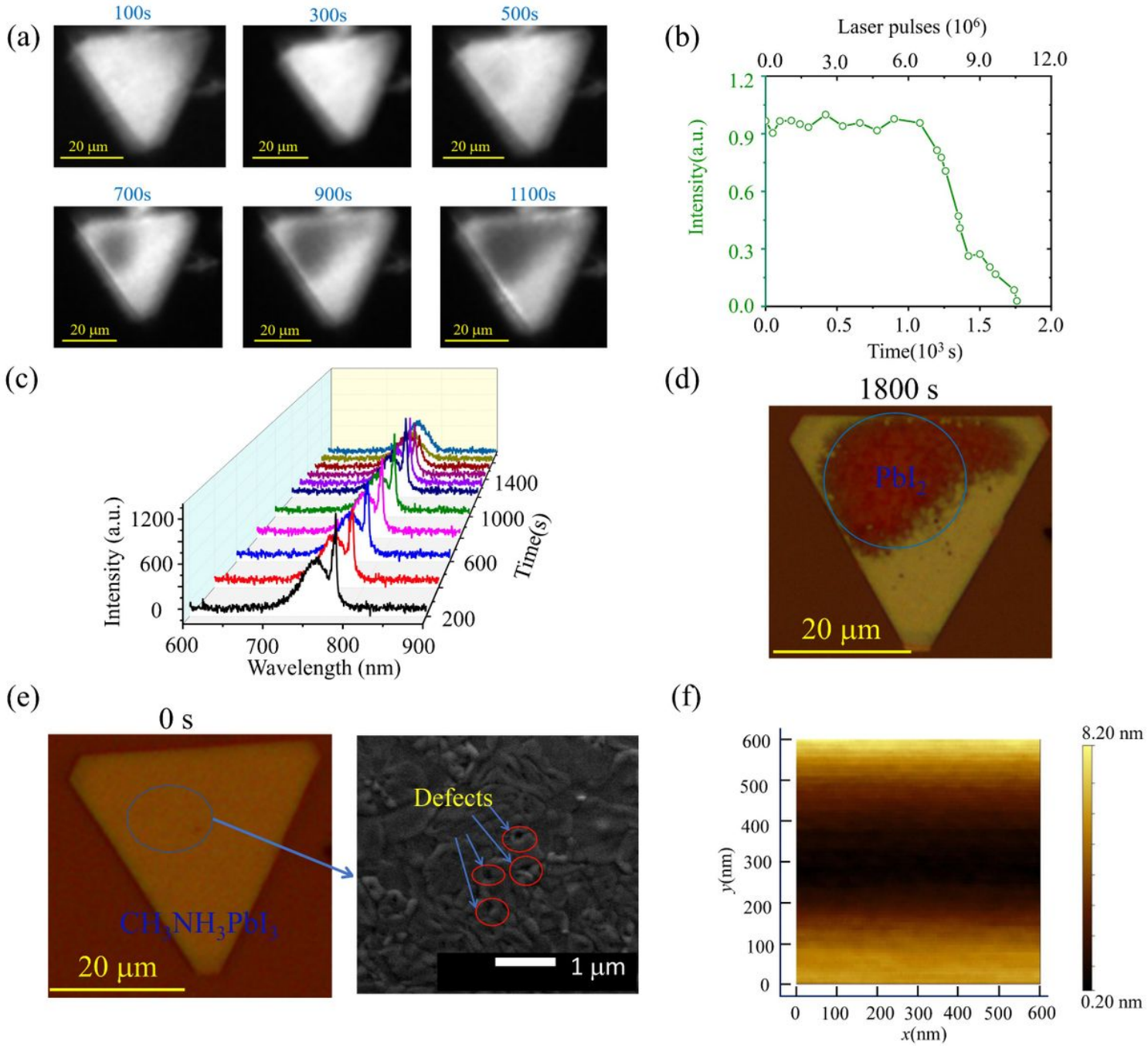

Figure 1

(a) Microscopic image of a $MAPbI_3$ laser operating at a pump density of $1.1P_{th}$ (26.1 mJ/cm^2) after working for different times. (b) Lasing stability data of $MAPbI_3$ laser under femtosecond laser pumping with a repetition rate of 6 kHz in ambient air condition. (c) Spectrum evolution of $MAPbI_3$ laser operating at a pump density of $1.1P_{th}$ (26.1 mJ/cm^2) after working for different times. (d) Microscopic image of the nanoplatelet after operating for 1800 s. (e) Microscopic image and SEM image of the initial $MAPbI_3$ nanoplatelet with surface defects. (f) Atomic force microscopic image of the $MAPbI_3$ nanoplatelet shows that its RMS roughness is 2.1 nm.

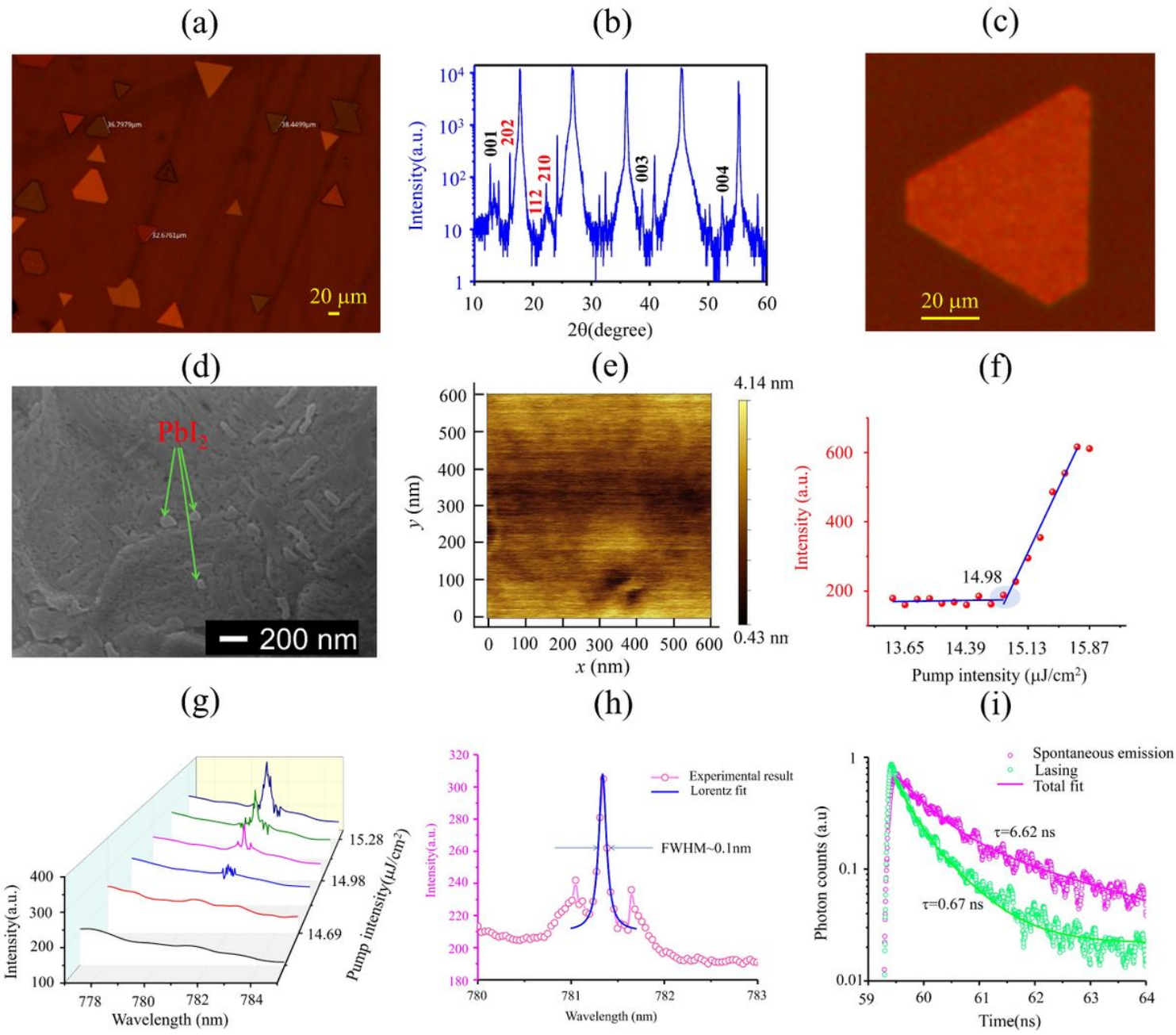

Figure 2

(a) Microscopic image of $MAPbI_3$ nanoplatelets on a mica substrate. (b) XRD pattern of the $MAPbI_3$ nanoplatelets. (c) Microscopic image of a $MAPbI_3$ nanoplatelet that used for demonstrating the laser before exposing to a pump laser. (d) SEM image of $MAPbI_3$ nanoplatelet. (e) AFM image of $MAPbI_3$ nanoplatelet shows its RMS roughness is ~ 0.7 nm. (f) Laser output intensity as a function of the pump density. (g) Evolution of emission spectra obtained at different pump densities. (h) Lorentz fitting of a lasing oscillation mode at ≈781.3 nm, gives a FWHM of 0.10 nm, corresponding to a Q factor of 7813. (i) Time-resolved photoluminescence (TRPL) spectra of perovskite nanoplatelet operating at spontaneous emission (P = 11.12 mJ/cm^2) and laser emission condition (P = 24.8 mJ/cm^2).

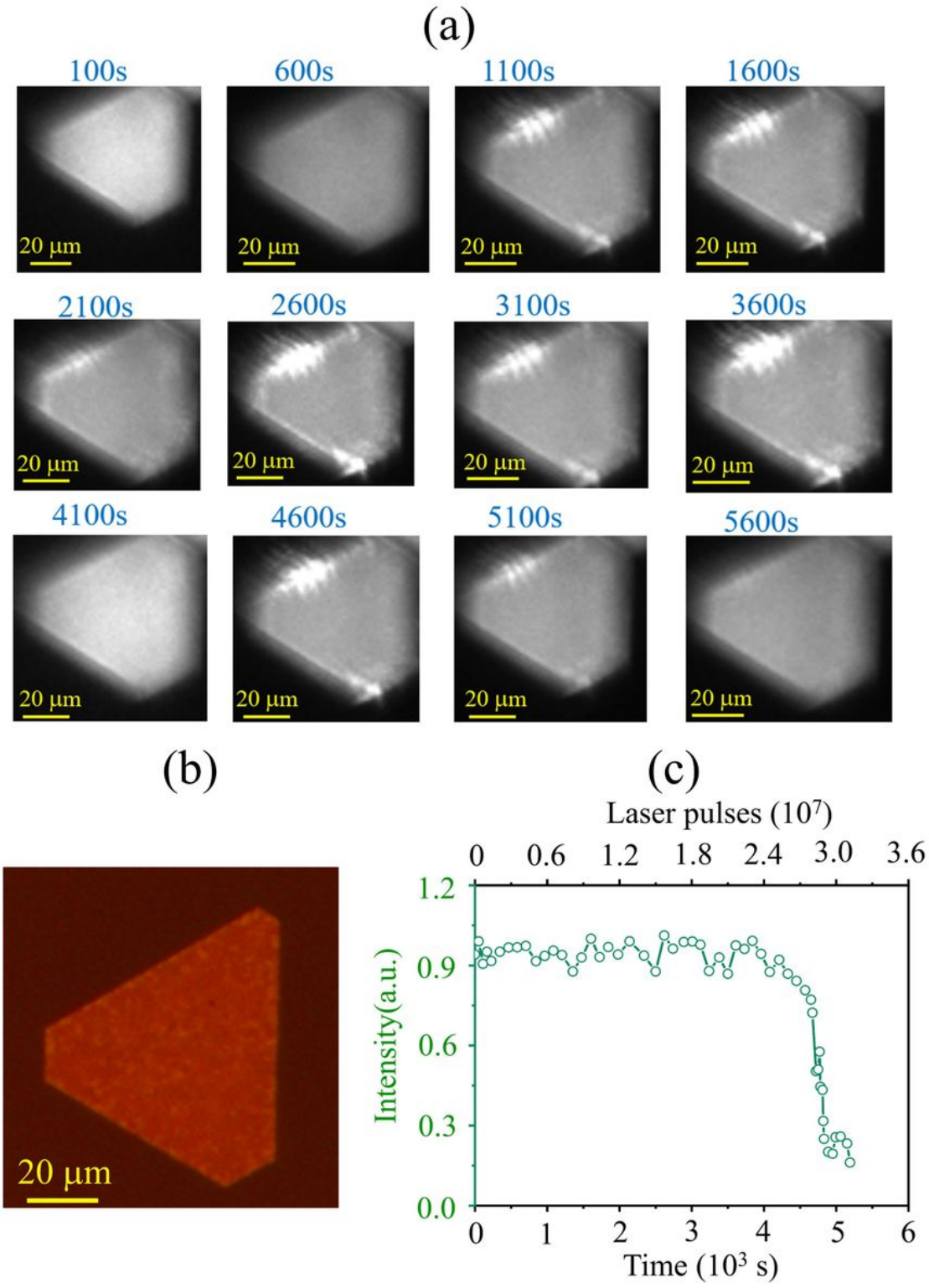

Figure 3

(a) Microscopic images of a PbI_2 passivated $MAPbI_3$ nanoplatelet laser by operating at a pump density of $1.1P_{th}$ (16.48 mJ/cm^2) for different times. (b) Microscopic image of $MAPbI_3$ nanoplatelet after operating at $1.1P_{th}$ for 5600 s. (c) Lasing stability data of PbI_2 passivated $MAPbI_3$ nanoplatelet under the femtosecond laser pumping with a repetition rate of 6 kHz in ambient air condition.

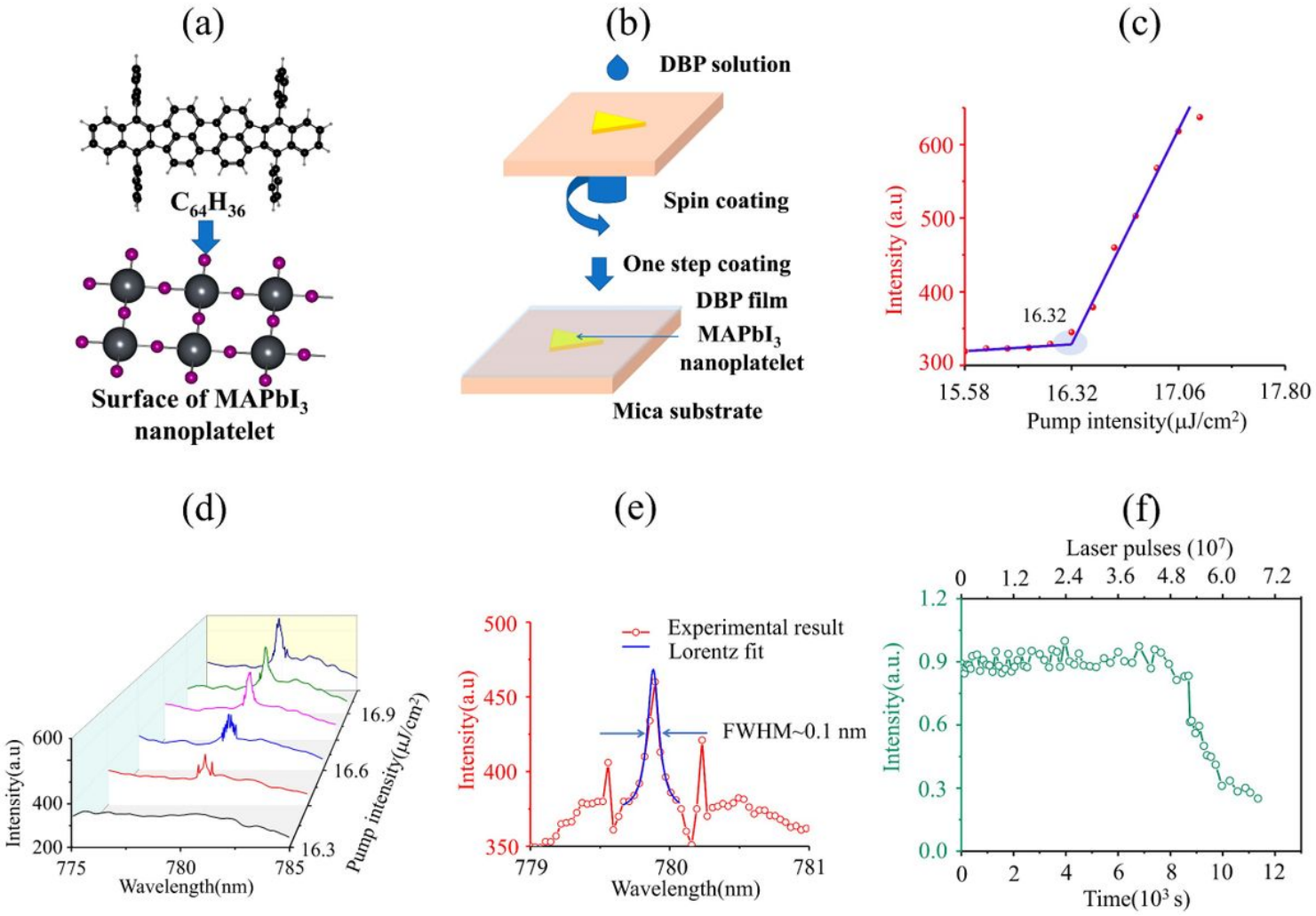

Figure 4

(a) Schematic diagram of passivating the surface of $MAPbI_3$ nanoplatelet with DBP ($C_{64}H_{36}$). (b) Process illustration of spin-coating a DBP film on the PbI_2 passivated $MAPbI_3$ nanoplatelet. (c) Laser output intensity as a function of pump density. (d) Evolution of emission spectra obtained at different pump densities. (e) Lorentz fitting of a lasing oscillation mode at ≈779.9 nm, gives a FWHM of 0.10 nm, corresponding to a Q factor of 7799. (f) Lasing stability data of the dual passivation processed $MAPbI_3$ nanoplatelet laser under the femtosecond laser pumping with a repetition rate of 6 kHz in ambient air condition. Dual passivation refers to PbI_2 passivation and DBP passivation.

Supplementary Files

This is a list of supplementary files associated with this preprint. Click to download.

- Supporting.docx